Am J Cancer Res 2023;13(4):1533-1546
www.ajcr.us /ISSN:2156-6976/ajcr0148748

Original Article

ZY-444 inhibits the growth and metastasis of prostate cancer by targeting TNFAIP3 through TNF signaling pathway

Meng-Ting Han[1,2*], Hua Pei[2*], Qi-Qi Sun[2], Cheng-Long Wang[2], Peng Li[3], Ya-Ya Xie[1], Li-Jun Cao[1], Xing-Xing Zhang[2], Zhen-Liang Sun[2]

[1]Anhui University of Science and Technology, Huainan 232001, Anhui, China; [2]Fengxian Hospital Affiliated to Anhui University of Science and Technology, Shanghai 201499, China; [3]State Key Laboratory of Quality Research in Chinese Medicine, Institute of Chinese Medical Sciences, University of Macau, Macao 999078, China. [*]Equal contributors.

Received December 25, 2022; Accepted April 6, 2023; Epub April 15, 2023; Published April 30, 2023

Abstract: Prostate cancer is one of the most lethal malignancies, and androgen deprivation therapy remains the mainstay of treatment for prostate cancer patients. Although androgen deprivation can initially come to remission, the disease often develops into castration-resistant prostate cancer (CRPC), which is still dependent on androgen receptor (AR) signaling and is related to a poor prognosis. Some success against CRPC has been achieved by drugs that target AR signaling, but secondary resistance uninterrupted emerges, and new therapies are urgently needed. In this study, we identified a potent small molecule compound, ZY-444, that suppressed PCa cells proliferation and metastasis, and inhibited tumor growth both in subcutaneous. Transcriptome sequencing analysis showed that TNFAIP3 was significantly elevated in prostate cancer cells after ZY-444 treatment. Further studies through overexpression of TNFAIP3 confirmed that TNFAIP3, as a direct target gene of ZY-444, contributes to the functions of ZY-444. In addition, we demonstrated the effects of TNFAIP3 on prostate cancer cell apoptosis, migration and proliferation to elucidate the mechanism of ZY-444. We found that TNFAIP3 inhibited the TNF signaling pathway, which could inhibit cell migration and proliferation and contribute to apoptosis. Overall, these findings highlighted TNFAIP3 as a tumor suppressor gene in the regulation of the progression and metastatic potential of prostate cancer and that targeting TNFAIP3 by ZY-444 might be a promising strategy for prostate cancer treatment.

Keywords: ZY-444, prostate cancer, metastasis, TNFAIP3, TNF signaling pathway

Introduction

Prostate cancer is a highly heterogeneous disease because of its complex etiology, which includes many environmental factors and phenotypic diversity that cause cellular process changes [1, 2], thus, prostate cancer patients will show a range of pathological entities with variable biological behavior and, consequently, different treatment modalities. In recent years, endocrine therapies have led to spectacular progress in prostate cancer therapy [3, 4]. Encouraging results have been observed with antiandrogen therapies and surgical treatment. Regrettably, a significant fraction of patients still progresses to castration-resistant prostate cancer (CRPC) and distant metastases and eventually succumb to the disease [5, 6]. Despite superior long-term survival in localized prostate cancer, metastatic disease remains largely incurable even after intensive multimodal therapy [7, 8]. There is thus an urgent need to develop novel, effective strategies for the treatment and prognosis of prostate cancer.

In previous studies, we found that ZY-444, a novel small-molecule compound, could inhibit tumor proliferation and metastasis through Wnt signaling pathway and bind to PC (pyruvate carboxylase), a key enzyme of tricarboxylic acid recycling, and reduce the basic respiration and ATP production of breast cancer cells [9]. In addition, as an inhibitor of PC, ZY-444 could effectively inhibit the activation of PC, reduce the malignant invasiveness, and restore the expression of iodine metabolism-related genes

and the iodine-uptake capacity in PTC cells [10]. Its lead compound KHS101, as an inhibitor of TACC3 signaling, can inhibit cell growth, motility, epithelial mesenchymal transformation, and induce cell death [11, 12]. ZY-444 also exhibited low toxicity to normal mammary epithelial cells. Prostate cancer and breast cancer are two common types of sex hormone-related cancers, and most patients eventually develop hormone-resistant malignancies after hormone deprivation [13]. Given the high potency of ZY-444 against breast cancer cells, ZY-444 was used to further investigate the cell function and tumorigenesis of prostate cancer in vitro and in vivo, as well as the mechanism by which ZY-444 might play a role in prostate cancer.

Materials and methods

Cell culture and compound treatment

PC3, DU145, C4-2 and 22RV1 cell lines were stored in the Cell Bank of Shanghai Key Laboratory of Regulatory Biology, East China Normal University. All prostate cancer cell lines were cultured in 10% fetal bovine serum with 1% penicillin/streptomycin and RPMI 1640 medium in an incubator at 37°C and 5% CO_2 under standard cell culture conditions. The small molecule compound ZY-444 was synthesized by Chen Yihua's research group at East China Normal University. ZY-444 was dissolved in DMSO to prepare a 1×10^4 μmol/L stock solution.

Cell proliferation assay

Briefly, after cells were conventionally cultured for 24 h, 10% The Cell Counting Kit-8 (CCK-8, Dojindo Laboratories, Minato-ku, Tokyo, Japan) was added, absorbance values at 450 nm were determined, and prostate cancer cell viability was measured by calculating the absorbance of Wells treated with ZY-444 or DMSO.

Apoptosis assay

Briefly, prostate cancer cells were seeded in 6-well plates with 4×10^5 cells/well, and after 24 h the cells were resuspended in cold phosphate-buffered saline (PBS), then operated according to the Annexin V-FITC Apoptosis Detection Kit (Becton Dickinson, Franklin Lakes, NH, USA) instructions, and they were analyzed by FACS (Becton Dickinson, Franklin Lakes, NJ, USA).

Clone formation assay

Prostate cancer cells (4×10^3 per well) were incubated with the specified concentration of the compound for 7 days, waiting for individual cells to proliferate and form a cell population, fixed with 4% paraformaldehyde for 20 min and stained with 0.2% crystal violet. Subsequently, cell colonies were washed with water and air-dried, and then images were taken using an inverted microscope.

Cell migration assay

The results were determined by wound healing and transwell migration assay. Briefly, confluence prostate cancer cells were starved overnight and scratched, cells were cultured in prescribed concentrations of compounds for 24 h, and migrating cells were microphotographed and counted manually. For the transwell migration assay, 5×10^4 cells were seeded in serum-free medium with the indicated concentration of the compound in the upper chamber. Medium containing serum was added to the bottom well of each chamber. After 24 h, nonmigrating cells in the upper chamber were removed by cotton swab, fixed with 4% paraformaldehyde and stained with 2% crystal violet. Images were obtained by taking pictures with an inverted microscope, and the number of migrating cells was manually counted.

Bioinformatic data mining

Prostate cancer PC3 cells were treated with high and low concentrations of ZY-444. After 24 h, cells RNA was extracted and collected for transcriptome gene sequencing. RNA sequencing was performed by Shanghai OE Biotech Co., LTD. According to the adjusted $P < 0.05$ and logarithmic change, mRNA with different expressions were selected for GO analysis and KEGG pathway significance analysis. Gene expression data of prostate cancer cases in the high-grade PCa UCSC Xena (http://xena.ucsc.edu/) data set, which includes 540 PCa tissues and 100 non-tumor tissues.

Plasmid construction and cell transfection

The full-length sequence of the human TNFAIP3 gene was purchased and subcloned into the

Table 1. The sequences of specific primers used for siTNFAIP3

Target Name	Target Sequence
siTNFAIP3 #1	S: GCGGAAAGCUGUGAAGAUATT
	AS: UAUCUUCACAGCUUUCCGCTT
siTNFAIP3 #2	S: GACACACGCAACUUUAAAUTT
	AS: AUUUAAAGUUGCGUGUGUCTT
siTNFAIP3 #3	S: CAGCAUGAGUACAAGAAAUTT
	AS: AUUUCUUGUACUCAUGCUGTT
siNC	S: UUCUCCGAACGUGUCACGUTT
	AS: ACGUGACACGUUCGGAGAATT

si, small interference; TNFAIP3, Tumor necrosis factor-α induced proteins 3; NC, negative control; S, sense; AS, antisense.

pCD513B vector (Geneppl Technology Co., Ltd.) with Lipofectamine 2000 (Invitrogen; Thermo Fisher Scientific, Inc.) according to the manufacturer's information, and the empty vector was used as the negative control. After 48 h, qPCR and Western blot were performed to test for subsequent validation experiments.

Transient transfection small interfering RNA (siRNA) and compound treatment

The TNFAIP3 gene-silenced plasmids (**Table 1**) were constructed (Shanghai GenePharma Co., Ltd.) to confirm the possibility of ZY-444 targeting the predicted TNFAIP3 gene. The 22RV1 cells were seeded onto 6-well plates at a density of 5×10^5 cells/ml per well and transfected with TNFAIP3 siRNA using Lipofectamine 2000. The siTNFAIP3 #1, siTNFAIP3 #2, siTNFAIP3 #3 and siNC (Suzhou Genepharma Co., Ltd.) were transfected into 22RV1 cells, following transfection for 48 h, qPCR and Western blot were performed to test whether TNFAIP3 gene was successfully silenced, and the sequence that was successfully silenced (siTNFAIP3 #3) was selected for subsequent validation experiments. For Western blot assay, the 22RV1 cells were first transfected with siTNFAIP3 along with their controls (siNC). Later, the transfected cells (siNC and siTNFAIP3) were treated with or without ZY-444 IC_{50} (2 μM in 22RV1) and incubated for 48 h at 37°C and 5% CO_2 to collect total proteins.

Western blot analysis

Total protein was extracted from the treated cells and animal tissues lysed with RIPA protein lysate containing 1 × protease inhibitor mixture (Roche Applied Science). The amount of total protein was quantified by BCA assay kit (Thermo Fisher) to obtain equal loads. Subsequently, lysates were fractionated on polyacrylamide gels and transferred to NC membrane. The blots were incubated with primary and secondary antibodies and the signals were visualized using a Tanon Highly-sig ECL Western Blotting Substrate Reagent Kit (#180-5001, Tanon Science and Technology Co., Ltd.). Then membranes were examined by the Tanon 4600 system. The primary antibodies to Bcl-2 (12789-1-AP; Proteintech), caspase-3 (66470-2-Ig; Proteintech), N-cadherin (22018-1-AP; Proteintech), Vimentin (10366-1-AP; Proteintech), E-cadherin (20874-1-AP; Proteintech), TNFAIP3 (23456-1-AP; Proteintech), RIPK1 (17519-1-AP; Proteintech), IKKα (AF6014; Affinity), IKBα (AF5002; Affinity) and p-IKBα (AF2002; Affinity), NF-κB (AF5006; Affinity), p-p65 (AF2006; Affinity) and β-actin (66009; Affinity). The secondary antibodies to HRP-conjugated Affinipure goat anti-mouse IgG (SA00001-1; Proteintech) and HRP-conjugated Affinipure goat anti-rabbit IgG (SA00001-2; Proteintech).

Animal studies

NOD-scid, male, 6-8-week-old mice were obtained from the Animal Center of East China Normal University. All animal experimental protocols were approved by the Animal Investigation Committee of the Institute of Biomedical Sciences, East China Normal University. DU145 cells (5×10^7) were suspended in PBS with 50% Matrigel and injected into the right flank of the mice. Treatment began after the tumor nodules reached 100-120 mm^3 in volume. The tumor-bearing mice were randomly assigned to four groups (n = 5-8) and treated with the indicated compounds. 1) DMSO vehicle; 2) 5 mg/kg/d ZY-444; 3) 2.5 mg/kg/d ZY-444; 4) 5 mg/kg/d Paclitaxel. All agents were administered via intraperitoneal injection (i.p.) daily. The tumor volume and mice body weight were measured after 6 days. The tumor volume (V) was calculated as length × width × width × 0.52. At the end of experiment, the mice were sacrificed. Solid tumors were removed and processed for immunohistochemistry analysis and pathological observation.

Immunohistochemistry and HE staining

Briefly, specimens of tumor tissue from xenograft models were fixed with 4% paraformalde-

Table 2. The sequences of specific primers used for Real-time quantitative PCR

Gene Name	Sequence (5'→3')
TNFAIP3	F: ATAGAAGATTCTAGAGCTAGCGCCACCATGGCTGAACAAGTCCTTCC R: GATCGCAGATCCTTCGCGGCCGCTTAGCCATCACATCTGCTTGA
β-actin	F: CATGTACGTTGCTACCCAGGC R: CTCCTTAATGTCACGGACGAT

TNFAIP3, Tumor necrosis factor-α induced proteins 3; F, forward; R, reverse.

hyde solution at 4°C overnight. Sections were stained overnight with antibodies Cleaved caspase-3 (AF7022; Affnity), Ki-67 (ab16667; Abcam) and TNFAIP3 (23456-1-AP, Proteintech) at 4°C, and they were performed using anti-rabbit or anti-mouse secondary antibody. Then, according to the manufacturer's instructions (SK-4100; Vector laboratories), the avidin-biotin peroxidase complex was used, followed by colorimetric detection using DAB. Formalin-fixed tissues were paraffin embedded, and 4-μm sections were prepared and stained with H&E. The sliced tissue slices were placed in a water bath at 40°C for spread, and the slices were baked in an oven at 60°C for 3 hours. Paraffin sections were deparaffinized with xylene and subjected to gradient ethanol hydration. Finally, hematoxylin was used to counterstain the sections and coverslips were mounted, and photographed using an inverted phase-contrast microscopy.

Real-time quantitative PCR (qPCR)

Total RNA for PCa cells were extracted with Trizol reagent (Takara, Japan) and reverse transcribed into cDNA using a cDNA reverse transcription kit (Takara, Japan). Real-time quantitative PCR was performed using a standard SYBR Green PCR kit (Thermo). All reactions were conducted using the following cycling parameters: 1 cycle for 2 min at 50°C; 40 cycles for 5 s at 95°C, 60°C for 30 s, respectively; with a final extension at 95°C for 15 s. β-actin was used as an endogenous control. The gene expression was analyzed using the $^{\Delta\Delta}$Ct method. The sequences of primers are shown as follows (**Table 2**).

Statistical analysis

Experiments were performed three or more replicates. Statistical analyses were determined by student's *t*-test. The differences between the control group and experimental groups were determined using one-way ANOVA. All analysis was performed using GraphPad Prism8. Data were presented as mean ± SD and $P < 0.05$ was considered significant.

Results

ZY-444 inhibits the proliferation of prostate cancer cells

In order to identify the inhibitory effect of small molecule compound ZY-444 (**Figure 1A**) on prostate cancer, we tested the efficacy of ZY-444 against the growth and viability of PCa cells, including C4-2, 22RV1, PC3, and DU145 cell lines. The growth curve and IC_{50} are shown in the **Figure 1B**. The semi-inhibitory concentrations of ZY-444 against these several cell lines ranged from 1.5 to 2.5 μmol/L. In colony formation, ZY-444 almost completely inhibited cell colony formation at the concentration of 5 μM compound (**Figure 1C**, **1D**). These results suggest that ZY-444 has a significant inhibitory effect on prostate cancer cells.

There is no doubt that induced apoptosis is one of the most effective strategies for prostate cancer. In presence of ZY-444 for 48 h, the numbers of apoptotic cells detected by flow cytometry analysis increased with rising dosage (**Figure 1E**, **1F**). Furthermore, we detected increases in apoptotic biomarkers caspase-3 and decreased expression of anti-apoptosis biomarkers Bcl-2 with ZY-444 treatment (**Figure 1G**). Thus, ZY-444 showed a noticeable inhibition of proliferation and induction of apoptosis on PCa cells.

ZY-444 inhibits PCa cell migration, metastasis and reverse the epithelial-to-mesenchymal transition (EMT) process

To further explore the effects of ZY-444 on the migration of PCa cells, wound healing assay and transwell migration assay were performed. The results indicated ZY-444 inhibitor cell migration (**Figure 2A-D**). In addition, a signifi-

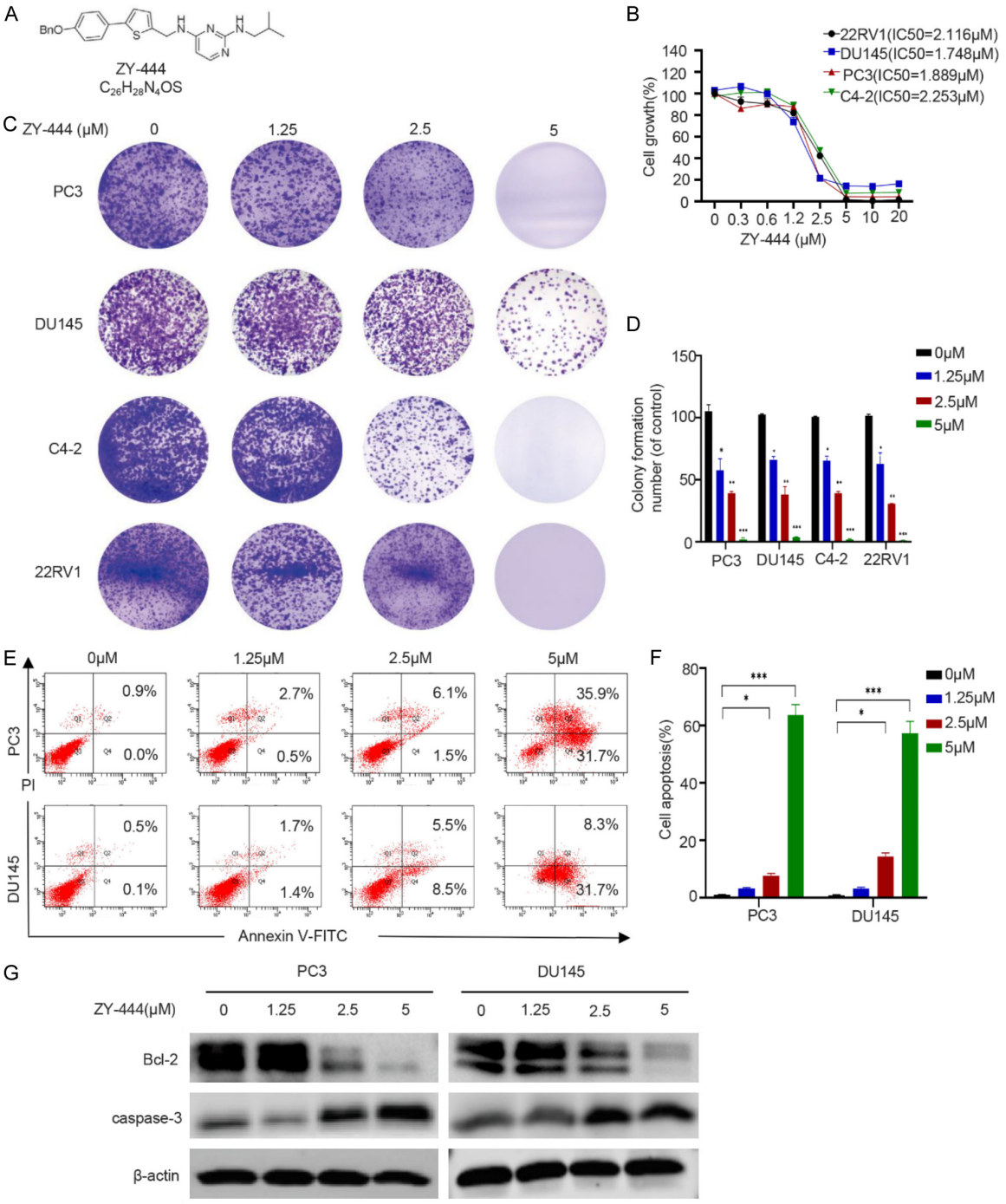

Figure 1. ZY-444 inhibits the proliferation of prostate cancer cells. A. The small-molecule compound structure of ZY-444. B. The effect of ZY-444 on cell growth. 22RV1, DU145, PC3 and C4-2 were treated with ZY-444 for 48 h, and the viability of cells was determined using the CCK-8 assay. C, D. The PC3, DU145, C4-2 and 22RV1 cell lines were treated with 0, 1.25, 2.5 or 5 μM ZY-444 in 6-well plates. After 7 days, cell colonies were counted, and colony formation for each cell line was presented. E, F. Cell apoptosis assays of PC3 and DU145 cells treated with NC or ZY-444 using FACS. Cells were collected and labeled with Annexin V-FITC and PI. G. Western blot analyses of caspase-3 and Bcl-2 treated with NC or ZY-444. β-actin was used as an internal control. *, $P < 0.05$; **, $P < 0.01$; ***, $P < 0.001$.

cantly increased expression of epithelial cadherin (E-cadherin) was noticed upon ZY-444 treatment. In contrast, the expression of neural cadherin (N-cadherin) and Vimentin were significantly decreased in both PCa cell line DU145 cells and PC3 cells (**Figure 2E**). The results

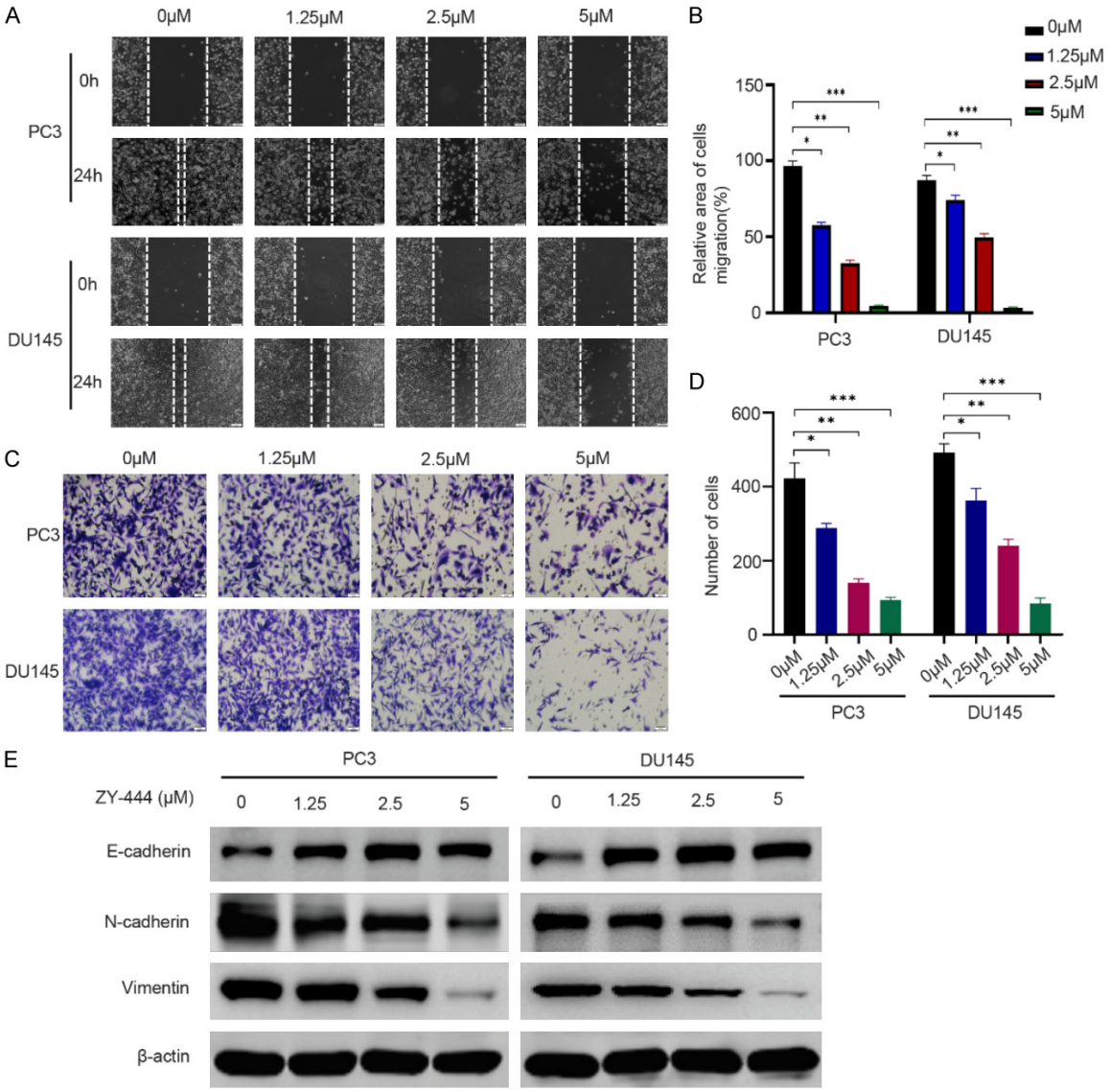

Figure 2. ZY-444 inhibits PCa cell migration and metastasis by inhibiting EMT-related proteins. A, B. PCa cells DU145 and PC3 were treated with 0, 1.25, 2.5 or 5 μM ZY-444, and wound healing assay was employed as described details in the methodology section. C, D. PCa cells DU145 and PC3 were treated with 0, 1.25, 2.5 or 5 μM ZY-444, and transwell migration assay was employed as described details in the methodology section. E. The PC3 and DU145 cells were treated with ZY-444 for 48 h; total protein was extracted and incubated with antibody (E-cadherin, N-cadherin and Vimentin) after executing Western blotting. β-actin was utilized as a control in Western blotting. *, $P < 0.05$; **, $P < 0.01$; ***, $P < 0.001$.

show that ZY-444 can suppress the EMT process by increasing E-cadherin and decreasing the expression of N-cadherin and Vimentin, thereby inhibiting the PCa cell migration and metastasis.

ZY-444 inhibits the growth of prostate cancer cells by targeting TNFAIP3

To explore the potential role of ZY-444 in prostate cancer, we selected high and low concentrations of ZY-444 for transcriptome sequencing in PC3 cells. Volcano map and heatmap showed the expression of TNFAIP3 in prostate cancer was obviously elevated (**Figure 3A**, **3B**), and pathway enrichment analysis showed that TNF signaling pathway was highly enriched (**Figure 3C**). To further confirm the association of TNFAIP3 with the expression of genes in prostate cancer and adjacent normal tissues, TNFAIP3 gene in clinical samples was further

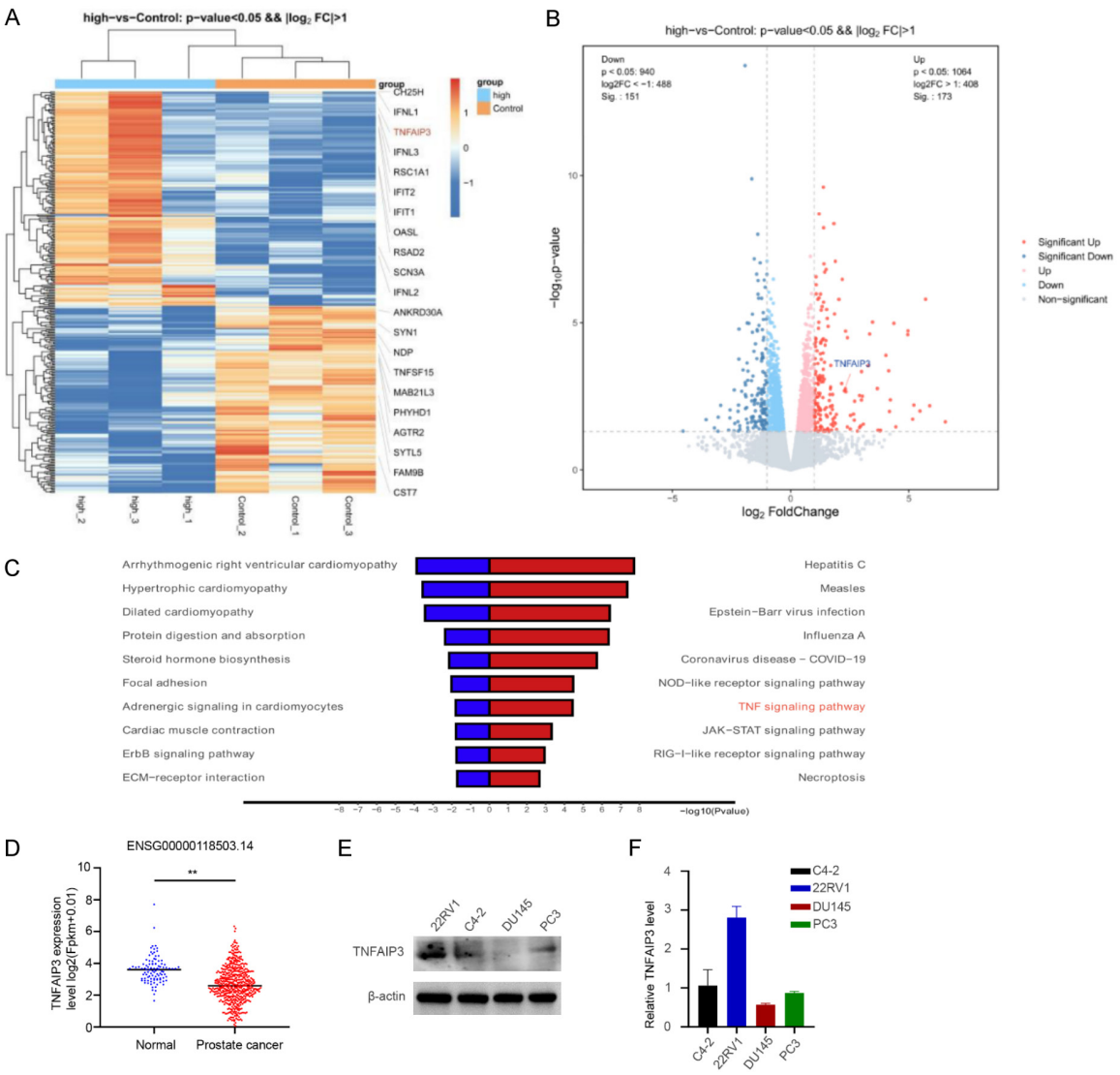

Figure 3. ZY-444 inhibits the growth of prostate cancer cells by targeting TNFAIP3. A. Heatmap analysis of gene expression in PC3 cells treated with ZY-444 or not (n = 3 holes per group). B. Volcano plots showed differentially expressed mRNAs. Gray indicates the mRNAs with nonsignificant differences; red and blue indicate those with significant differences. C. KEGG enrichment analysis was performed on the upregulated and downregulated differentially expressed mRNAs. D. UCSC data analysis of the expression of TNFAIP3 in prostate cancer and adjacent normal tissues. E, F. The expression levels of TNFAIP3 in PCa cell lines were assessed by Western blot and qPCR. **, P < 0.01.

verified and analyzed using UCSC Xena (http://xena.ucsc.edu/). The UCSC data showed that the expression of TNFAIP3 in prostate cancer was lower than that in adjacent normal tissues (**Figure 3D**).

In addition, the expression levels of TNFAIP3 were further detected in several PCa cell lines by qPCR and Western blot. Among all PCa cell lines examined, 22RV1 cells exhibited the highest TNFAIP3 expression levels, while PC3 and DU145 cells were relatively lower (**Figure 3E**, **3F**). Therefore, PC3 and DU145 cells were selected for the subsequent overexpression experiments, and 22RV1 cells were selected for knockdown experiments. Furthermore, the transfection efficiency of TNFAIP3 in PCa cells was also verified (Figure S1A-E).

ZY-444 inhibits prostate cancer cell growth and affects the TNF signaling pathway in vivo

To determine the anti-tumor activities of ZY-444 in vivo, DU145 xenograft model was used. As

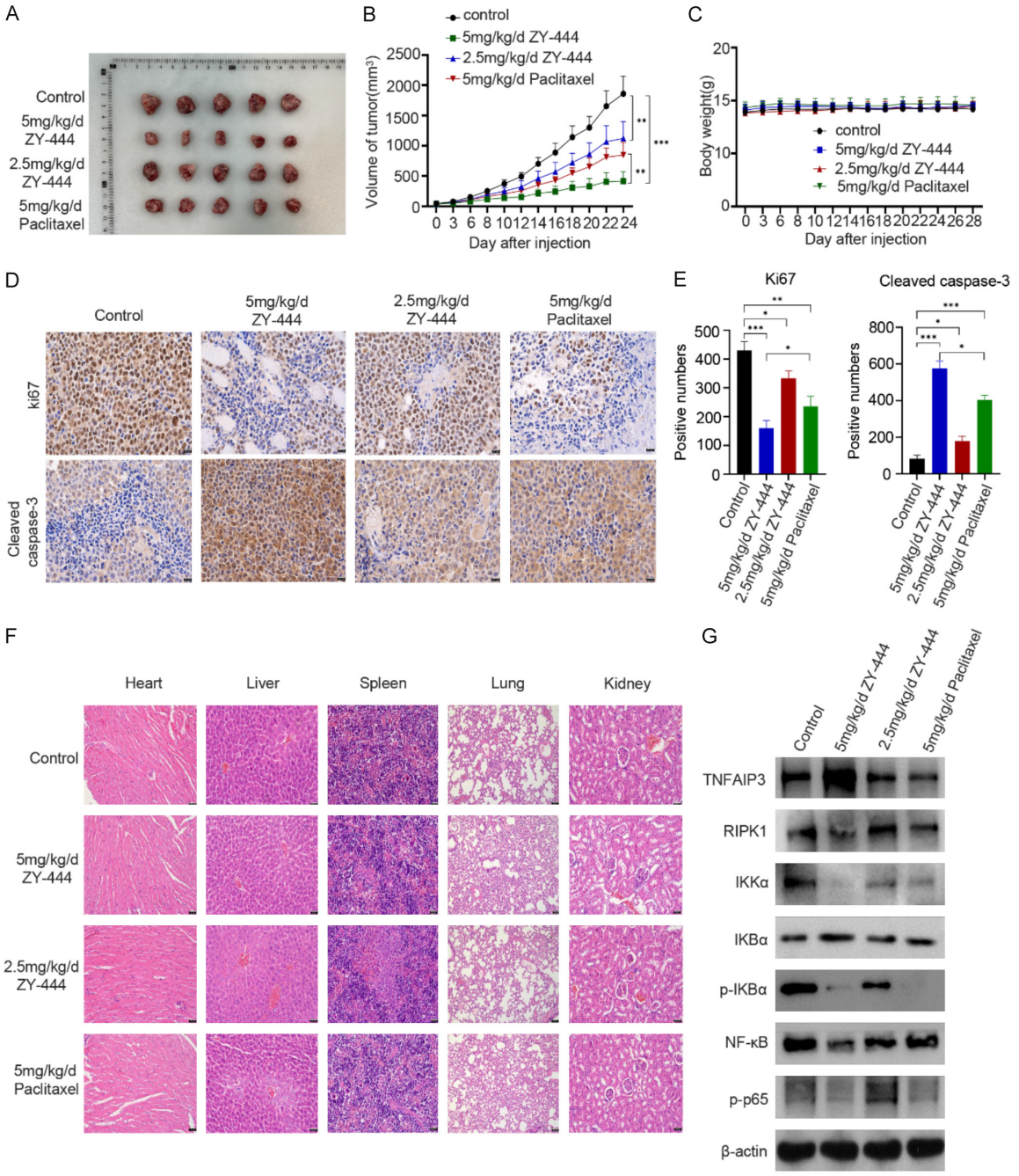

Figure 4. ZY-444 inhibits prostate cancer cell growth and affects the TNF signaling pathway in vivo. A. DU145 tumor-bearing NOD-scid mice were treated with ZY-444 at 2.5 and 5 mg/kg/d, Pacitaxel at 5 mg/kg/d or with control. Compared to the control group, ZY-444 and Pacitaxel-treated group showed inhibition of tumor growth. B. Tumor volumes were measured three per week, and treatment with ZY-444 resulted in significant inhibition of tumor volume compared to treatment with the control. C. ZY-444 did not cause obvious changes in body weight in the control and ZY-444-treated groups. D. IHC staining analysis and protein expression of Ki-67, Cleaved caspase-3 expression in tumors. The scale bar denotes 20 μm. E. The quantification of Ki67 and Cleaved caspase-3 immunostaining. F. ZY-444 (2.5 mg/kg/d and 5 mg/kg/d) did not cause obvious pathological abnormalities in normal tissues. H&E staining of paraffin-embedded sections of the heart, liver, spleen, heart, lung and kidney. G. ZY-444 affected the expression of genes related to TNF signaling pathway (n = 5, *, $P < 0.05$; **, $P < 0.01$; ***, $P < 0.001$).

shown in **Figure 4A**, **4B**, ZY-444 was more effective in inhibiting tumor growth compared with paclitaxel at the same dose. Importantly, no significant differences in body weights were

found among the ZY-444 treatment groups and DMSO control group (**Figure 4C**). Moreover, at the higher dose, a significant increase in cleaved caspase-3 was observed, which provided evidence for ZY-444-induced apoptosis in vivo. As additional markers of proliferation, the Ki-67 expression was also examined, and administration of ZY-444 significantly inhibited Ki-67 expression in DU145 xenograft model (**Figure 4D**, **4E**). Furthermore, toxic pathologic changes in the hearts, livers, spleens, lungs, and kidneys were not detected by H&E staining (**Figure 4F**). These data suggested that the inhibition of tumor growth by ZY-444 was not attributable to systemic toxicity.

In addition, in order to verify the mechanism of ZY-444 inhibits the progression and metastatic potential of prostate cancer in vivo, we detected the expression of TNF signaling pathway related genes through Western blot assay. As expected, ZY-444 of 5 mg/kg/d significantly inhibited the expression of RIPK1, IKKα, p-Ikkα and NF-κB, and increased the expression of TNFAIP3 and inhibitor IKBα compared with the control group and the low concentration group (**Figure 4G**). These results together indicated that ZY-444 impaired TNF signaling through inducing TNFAIP3.

TNFAIP3 inhibits proliferation, migration and induces apoptosis of prostate cancer cells

To further uncover the potential role of TNFAIP3 in PCa, PC3 and DU145 cell lines were transfected with overexpression of TNFAIP3 or siTNFAIP3 transfected in 22RV1. Following cell transfection for 48 h, the cell proliferation ability was assessed by CCK-8. The results indicated that compared with the control, overexpression of TNFAIP3 significantly inhibited cell proliferation in a time-dependent manner (**Figure 5A**, **5B**), In contrast, significantly promoted the proliferation were found upon siTNFAIP3 transfection compared to NC group in 22RV1 cell lines (**Figure 5C**). The flow cytometry confirmed that TNFAIP3 overexpression induced apoptosis in prostate cancer cells compared with the NC group transfected with TNFAIP3 (Figure S2A, S2B). Then, expression of the apoptosis-related protein was measured by Western blot, such as caspase-3 and Bcl-2 (Figure S2C). The results indicated that TNFAIP3 increased pro-apoptosis protein expression and decreased anti-apoptosis protein expression.

Similarly, wound healing assay and transwell migration assay in overexpressed cell lines indicated overexpression of TNFAIP3 inhibited cell migration (**Figure 5D-G**). However, the silencing of TNFAIP3 was found to have significantly enhanced cell migration rates and the healing action in 22RV1 cells (**Figure 5H-K**). In summary, the effect of TNFAIP3 is consistent with a tumor-suppressive function of ZY-444 treatment.

TNFAIP3 inhibits the epithelial-mesenchymal transition (EMT) of PCa cells

We further verified the influence of TNFAIP3 on the expression of E-cadherin, N-cadherin and Vimentin proteins in epithelial cell characteristics through overexpression or knockdown. A significantly increased expression of E-cadherin was noticed with overexpression of TNFAIP3 transfection in PC3 and DU145 cells lines, while the expression of N-cadherin and Vimentin were significantly decreased (**Figure 5L**). In contrary, siTNFAIP3 significantly decreased E-cadherin and increased N-cadherin and Vimentin in the 22RV1 cell lines (**Figure 5M**). The results showed that TNFAIP3 could reverse the epithelial-to-mesenchymal transition process of prostate cancer cells, thereby inhibiting cell migration and metastasis.

ZY-444 affects TNF signaling by targeting TNFAIP3

As described above, TNFAIP3 is target gene of ZY-444 treatment for PCa cells, but the mechanism of the effect of TNFAIP3 still needs to be studied in PCa cells. Previous studies have shown that the zinc-finger protein TNFAIP3 has dual physiological functions of inhibiting nuclear factor-κB (NF-κB) activation and apoptosis in tumor necrosis factor (TNF) receptor 1 signaling pathway [14]. When the TNF pathway is activated, TNF binds to TNFR1 (TNF receptor 1) to induce the recruitment of TNF receptor-associated death domain protein (TRADD) and receptor interacting protein 1 (RIPK1), activate IKK complex, IKKα phosphorylates IKBα, and ubiquitination and proteasomal degradation through K48 ligation assay [15-17]. The P50/P65 NF-κB dimer is released, which transfer to the nucleus and induces expression of NF-κB responsive genes [18]. TNFAIP3 was shown to negatively regulate NF-κB signaling by replacing K63-linked chains on RIPK1 with K48-linked

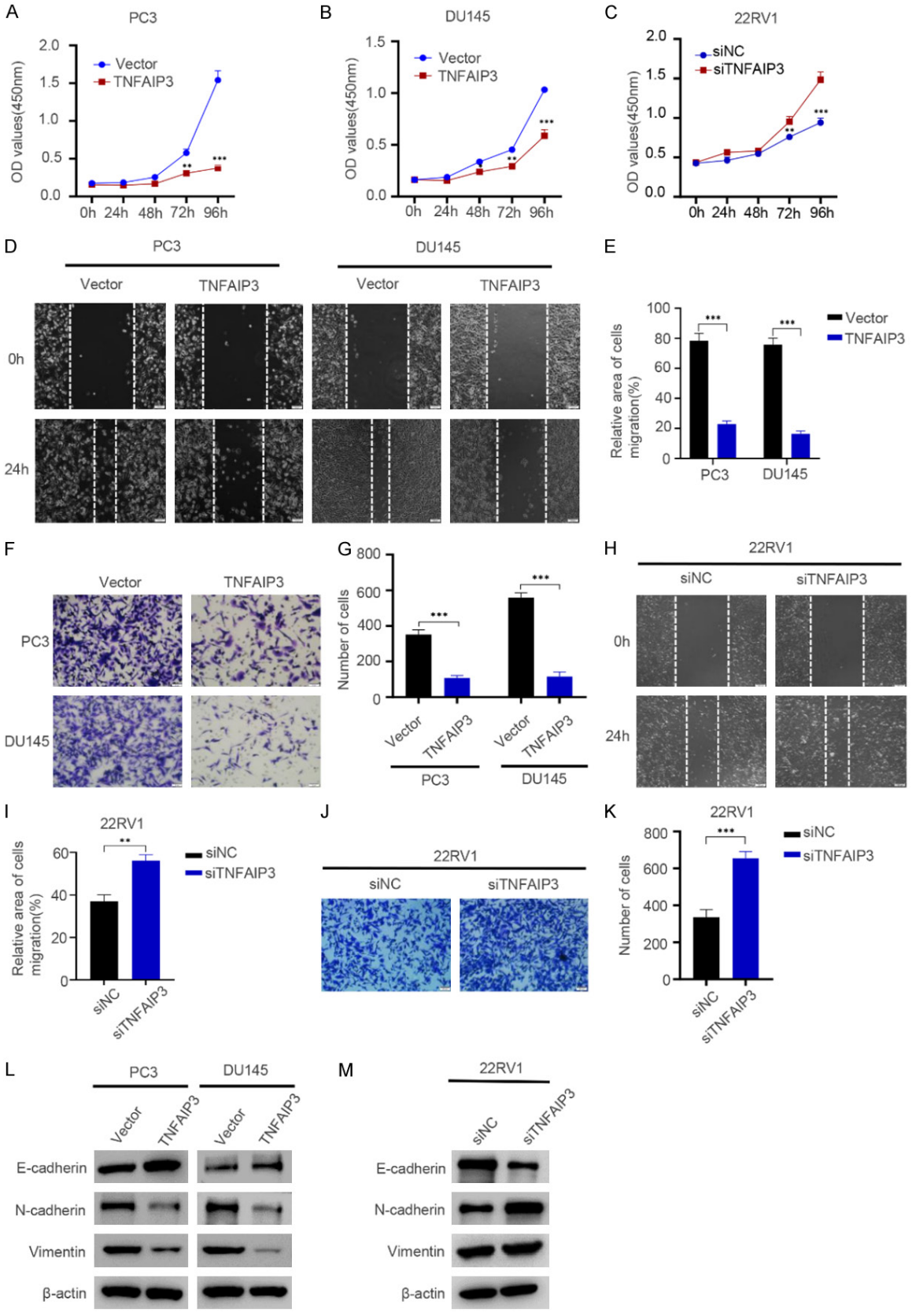

Figure 5. TNFAIP3 inhibits proliferation and migration of prostate cancer cells. A, B. CCK-8 was used to assess the proliferation of PC3 and DU145 cells transfected with over-expression of TNFAIP3 at 0 h, 24 h, 48 h, 72 h and 96

h. C. CCK-8 was used to assess the proliferation of 22RV1 cells transfected with siTNFAIP3 at 0 h, 24 h, 48 h, 72 h and 96 h. D, E. Wound healing assays of PC3 and DU145 cells after transfection with over-expression of TNFAIP3. F, G. Transwell migration assays of PC3 and DU145 cells after transfection with over-expression of TNFAIP3. H, I. Wound healing assays of 22RV1 cells after transfection with siTNFAIP3. J, K. Transwell migration assays of 22RV1 cells after transfection with siTNFAIP3. L. Western blot analyses of E-cadherin, N-cadherin and Vimentin in PC3 and DU145 cells after transfection with over-expression of TNFAIP3. β-actin was used as an internal control. M. Western blot analyses of E-cadherin, N-cadherin and Vimentin in 22RV1 cells after transfection with siTNFAIP3. β-actin was used as an internal control. **, P < 0.01; ***, P < 0.001.

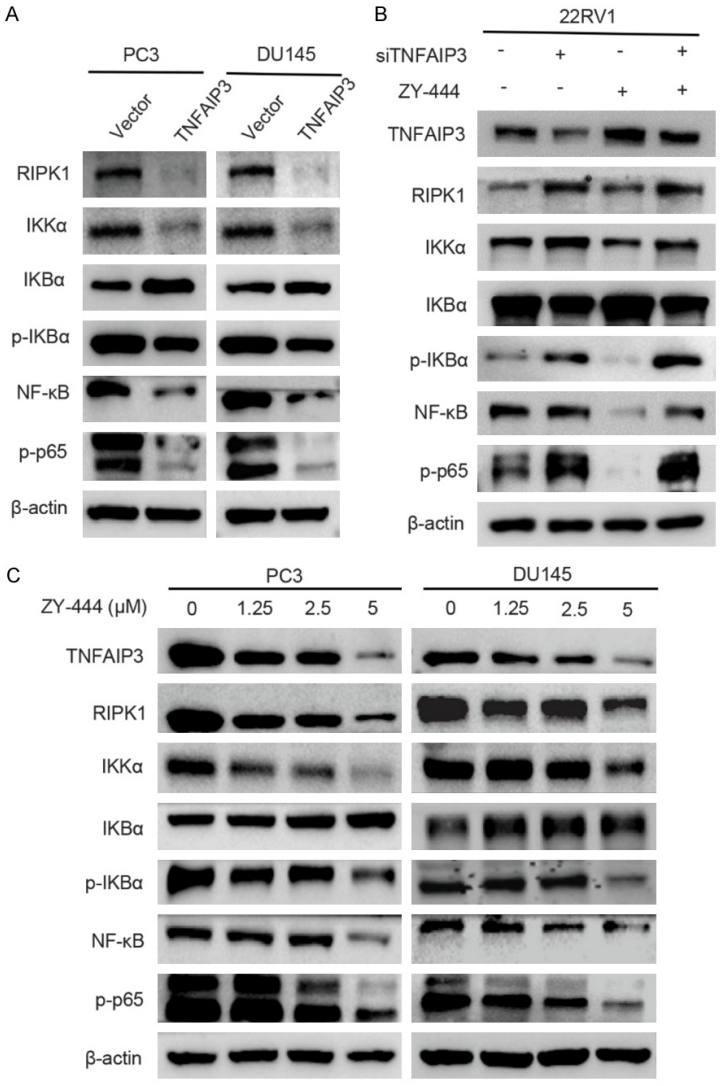

Figure 6. ZY-444 affects TNF signaling by targeting TNFAIP3. A. TNF signaling factors were assessed. β-actin served as a loading control after transfection with over-expression of TNFAIP3. B. The 22RV1 cells were transfected or treated with siTNFAIP3 and ZY-444 IC_{50} individually or combined, and for Western blotting, proteins associated with TNF signaling pathway were detected. As a control, β-actin was employed. C. TNF signaling factors were assessed treated with 0, 1.25, 2.5 or 5 μM ZY-444. β-actin served as a loading control.

chains, which targeted RIPK1 for proteasomal degradation [19]. In this study, we found that TNFAIP3 inhibits expression of RIPK1, IKKα, p-IKBα and NF-κB. Increased expression of repressor IKBα (**Figure 6A**), suggesting that TNFAIP3 exerts its anticancer effect in prostate cancer mainly by inhibiting the TNF signaling pathway.

We inquired into the possibility of knockdown of TNFAIP3 in the TNF activation and its involvement in ZY-444-mediated TNF activation. We performed knockdown of TNFAIP3 together with or without ZY-444 treatment in the 22RV1 cell lines. The data from Western blotting showed that there was a significantly increased RIPK1, IKKa, p-IkBa, NF-κB and p-p65 in siTNFAIP3 22RV1 cells but decreased IkBa compared to NC group and thereby upregulating the TNF activation, while the opposite results were found in ZY-444 treatment. However, their combination treatment could reverse that ZY-444 inhibited the production of TNF signaling (**Figure 6B**). Meanwhile, we observed that ZY-444 treatment of prostate cancer cells also inhibited or promoted the expression of these genes in a concentration-dependent manner (**Figure 6C**). The aforementioned findings indicated that ZY-444 inhibited the progression and metastatic of prostate cancer by affecting the TNF signaling pathway.

Discussion

The American Cancer Society (ACS) showed that the estimated new cases of prostate cancer ranked first in male incidence and became the most common form of malignant tumor [20]. Currently, the treatment for PCa patients is

mainly endocrine therapy [21], radiotherapy [22], chemotherapy and new therapy such as tumor vaccine and cryotherapy [23, 24], but usually, these face severe challenges such as poor efficacy, complications, and drug resistance. Therefore, developing a new and effective therapeutics for prostate cancer is urgently. Our findings introduce a small molecule, ZY-444, with potent anti-prostate cancer growth effect in vitro and in vivo.

In this study, we investigated the molecular mechanism that the small molecular compound ZY-444 uses to regulate the growth and metastasis of PCa cells. We found that ZY-444 significantly inhibited the growth and migration process of the PCa cells, induced apoptosis, and reversed the EMT phenotype in a concentration-dependent manner. In addition, we constructed a subcutaneous tumor growth xenograft model that inhibited the growth of cancer cells in vivo after treating mice with ZY-444. Transcriptional genomics analysis, and a Western blot indicated the molecular mechanism of ZY-444 against prostate cancer, proving that TNFAIP3 was a critical target for ZY-444 action. More importantly, UCSC data showed that the expression of TNFAIP3 in prostate cancer was lower than that in adjacent normal tissues. ZY-444 inhibited the growth and metastasis of PCa cells by downregulating the protein levels of RIPK1, IKKα, p-IKBα and NF-κB. The abovementioned results showed that the small molecular compound ZY-444 significantly inhibited PCa cell growth and metastasis, and promoted cancer cells apoptosis. Those targeted genes that were coupled with TNF signaling as the core can be used for ZY-444 therapy, with TNFAIP3 as the critical targets for regulation, thus laying the foundation and possibility for their use in the targeted therapy of PCa.

As one of the members of the TNF superfamily, the role of TNFAIP3 as a tumor suppressor was first discovered in B cell lymphomas [25]. Subsequent studies revealed the dual roles of TNFAIP3 in solid cancers [26]. Re-expression of TNFAIP3 in TNFAIP3-deficient lymphoma cell lines resulted in cell apoptosis and growth arrest accompanied by downregulation of NF-κB signaling [27]. Deletion of TNFAIP3 in intestinal epithelial cells and myeloid cells cause development of colorectal tumors in aged mice, enhancing the apoptosis of IEC exposed to inflammatory cytokines or carcinogens [28, 29]. The overexpression of TNFAIP3 can significantly inhibit the proliferation, metastasis, and invasion of hepatocellular carcinoma cells in vitro, and the tumor suppressive effect of TNFAIP3 was also demonstrated in vivo [30, 31]. However, TNFAIP3 acts as an oncogenic regulator in breast cancers [32], gastric cancers [33] and melanomas [34], indicating that TNFAIP3 acts as an oncogenic factor in these cancers. Therefore, TNFAIP3 may play different roles in different cancers. In this study, TNFAIP3 was up-regulated in the ZY-444-treated PCa cells, thus acting as a tumor suppressor. Similarly, we used gene overexpression assays the TNFAIP3 mRNA expression. The results showed that the PC3 and DU145 cells that were transfected with a TNFAIP3 overexpression plasmid had significantly inhibited growth and metastasis ability when they were compared with the PCa cells with empty plasmid transfection, however, the proliferation and migration abilities of 22RV1 cells were significantly increased following cell transfection with siTNFAIP3 compared with the corresponding NC group. In addition, this study also examined the effects of silenced TNFAIP3 in the reversal of ZY-444 inhibition on TNF. We determined that the expression of TNF signaling pathway related genes when 22RV1 cells were treated with ZY-444 and siTNFAIP3, the TNF signaling pathway was reactivated compared to ZY-444 alone. In conclusion, ZY-444 inhibited the progression and metastatic potential of prostate cancer by targeting TNFAIP3 through TNF signaling pathway.

In summary, ZY-444 has significant anti-PCa activity. Target molecule TNFAIP3 play a vital role in regulating cell proliferation, apoptosis and migration through the TNF signaling pathway, and it can be used as a biomarker for the treatment of PCa by the ZY-444. TNFAIP3 serve as key regulatory targets of ZY-444, this providing new compounds and candidate targets for the clinical treatment of PCa.

Acknowledgements

Thanks to Professor Yihua Chen of East China Normal University for sending the small molecule compound ZY-444. We would like to express our sincere thanks to the Animal Center of East China Normal University for providing the experimental platform. This work was supported by the grants from the National Natural

Science Foundation of China (81872418), and Science and Technology Commission of Shanghai Municipality (21S11902000), and Shanghai Fengxian District Science and Technology Project (2023).

Disclosure of conflict of interest

None.

Address correspondence to: Xing-Xing Zhang and Zhen-Liang Sun, Fengxian Hospital Affiliated to Anhui University of Science and Technology, Shanghai 201499, China. Tel: +86-021-57423428; E-mail: simonzx1989@163.com (XXZ); Tel: +86-021-57416150; E-mail: zhenliang6@126.com (ZLS)

References

[1] Haffner MC, Zwart W, Roudier MP, True LD, Nelson WG, Epstein JI, De Marzo AM, Nelson PS and Yegnasubramanian S. Genomic and phenotypic heterogeneity in prostate cancer. Nat Rev Urol 2021; 18: 79-92.

[2] Deutsch E, Maggiorella L, Eschwege P, Bourhis J, Soria JC and Abdulkarim B. Environmental, genetic, and molecular features of prostate cancer. Lancet Oncol 2004; 5: 303-313.

[3] Di Donato M, Zamagni A, Galasso G, Di Zazzo E, Giovannelli P, Barone MV, Zanoni M, Gunelli R, Costantini M, Auricchio F, Migliaccio A, Tesei A and Castoria G. The androgen receptor/filamin A complex as a target in prostate cancer microenvironment. Cell Death Dis 2021; 12: 127.

[4] AR blockers augment other cancer treatments. Cancer Discov 2022; 12: OF2.

[5] Cheng WL, Huang CY, Tai CJ, Chang YJ and Hung CS. Maspin enhances the anticancer activity of curcumin in hormone-refractory prostate cancer cells. Anticancer Res 2018; 38: 863-870.

[6] Li Y and Cozzi PJ. Targeting uPA/uPAR in prostate cancer. Cancer Treat Rev 2007; 33: 521-527.

[7] Martel CL, Gumerlock PH, Meyers FJ and Lara PN. Current strategies in the management of hormone refractory prostate cancer. Cancer Treat Rev 2003; 29: 171-187.

[8] Wang G, Zhao D, Spring DJ and DePinho RA. Genetics and biology of prostate cancer. Genes Dev 2018; 32: 1105-1140.

[9] Lin Q, He Y, Wang X, Zhang Y, Hu M, Guo W, He Y, Zhang T, Lai L, Sun Z, Yi Z, Liu M and Chen Y. Targeting pyruvate carboxylase by a small molecule suppresses breast cancer progression. Adv Sci (Weinh) 2020; 7: 1903483.

[10] Liu Y, Liu C, Pan Y, Zhou J, Ju H and Zhang Y. Pyruvate carboxylase promotes malignant transformation of papillary thyroid carcinoma and reduces iodine uptake. Cell Death Discov 2022; 8: 423.

[11] Campo L and Breuer EK. Inhibition of TACC3 by a small molecule inhibitor in breast cancer. Biochem Biophys Res Commun 2018; 498: 1085-1092.

[12] Wang J, Du S, Fan W, Wang P, Yang W and Yu M. TACC3 as an independent prognostic marker for solid tumors: a systematic review and meta-analysis. Oncotarget 2017; 8: 75516-75527.

[13] Wang X, Fang Y, Sun W, Xu Z, Zhang Y, Wei X, Ding X and Xu Y. Endocrinotherapy resistance of prostate and breast cancer: importance of the NF-κB pathway (review). Int J Oncol 2020; 56: 1064-1074.

[14] Won M, Park KA, Byun HS, Sohn KC, Kim YR, Jeon J, Hong JH, Park J, Seok JH, Kim JM, Yoon WH, Jang IS, Shen HM, Liu ZG and Hur GM. Novel anti-apoptotic mechanism of A20 through targeting ASK1 to suppress TNF-induced JNK activation. Cell Death Differ 2010; 17: 1830-1841.

[15] Liu J, Zhu Z, Wang L, Du J, Zhang B, Feng X and Zhang G. Functional suppression of Ripk1 blocks the NF-κB signaling pathway and induces neuron autophagy after traumatic brain injury. Mol Cell Biochem 2020; 472: 105-114.

[16] Martens A and van Loo G. A20 at the crossroads of cell death, inflammation, and autoimmunity. Cold Spring Harb Perspect Biol 2020; 12: a036418.

[17] Shen J, Cheng J, Zhu S, Zhao J, Ye Q, Xu Y, Dong H and Zheng X. Regulating effect of baicalin on IKK/IKB/NF-kB signaling pathway and apoptosis-related proteins in rats with ulcerative colitis. Int Immunopharmacol 2019; 73: 193-200.

[18] Momtazi G, Lambrecht BN, Naranjo JR and Schock BC. Regulators of A20 (TNFAIP3): new drug-able targets in inflammation. Am J Physiol Lung Cell Mol Physiol 2019; 316: L456-L469.

[19] Wertz IE, O'Rourke KM, Zhou H, Eby M, Aravind L, Seshagiri S, Wu P, Wiesmann C, Baker R, Boone DL, Ma A, Koonin EV and Dixit VM. De-ubiquitination and ubiquitin ligase domains of A20 downregulate NF-kappaB signalling. Nature 2004; 430: 694-699.

[20] Siegel RL, Miller KD, Fuchs HE and Jemal A. Cancer statistics, 2022. CA Cancer J Clin 2022; 72: 7-33.

[21] Damber JE. Endocrine therapy for prostate cancer. Acta Oncol 2005; 44: 605-609.

[22] Wallis CJD, Saskin R, Choo R, Herschorn S, Kodama RT, Satkunasivam R, Shah PS, Danjoux C and Nam RK. Surgery versus radiotherapy for clinically-localized prostate cancer: a systematic review and meta-analysis. Eur Urol 2016; 70: 21-30.

[23] Sutherland SIM, Ju X, Horvath LG and Clark GJ. Moving on from Sipuleucel-T: new dendritic cell vaccine strategies for prostate cancer. Front Immunol 2021; 12: 641307.
[24] Jung JH, Risk MC, Goldfarb R, Reddy B, Coles B and Dahm P. Primary cryotherapy for localised or locally advanced prostate cancer. BJU Int 2019; 124: 383-385.
[25] Kato M, Sanada M, Kato I, Sato Y, Takita J, Takeuchi K, Niwa A, Chen Y, Nakazaki K, Nomoto J, Asakura Y, Muto S, Tamura A, Iio M, Akatsuka Y, Hayashi Y, Mori H, Igarashi T, Kurokawa M, Chiba S, Mori S, Ishikawa Y, Okamoto K, Tobinai K, Nakagama H, Nakahata T, Yoshino T, Kobayashi Y and Ogawa S. Frequent inactivation of A20 in B-cell lymphomas. Nature 2009; 459: 712-716.
[26] Shi Y, Wang X, Wang J, Wang X, Zhou H and Zhang L. The dual roles of A20 in cancer. Cancer Lett 2021; 511: 26-35.
[27] Shembade N and Harhaj EW. Regulation of NF-κB signaling by the A20 deubiquitinase. Cell Mol Immunol 2012; 9: 123-130.
[28] Rusu I, Mennillo E, Bain JL, Li Z, Sun X, Ly KM, Rosli YY, Naser M, Wang Z, Advincula R, Achacoso P, Shao L, Razani B, Klein OD, Marson A, Turnbaugh JA, Turnbaugh PJ, Malynn BA, Ma A and Kattah MG. Microbial signals, MyD88, and lymphotoxin drive TNF-independent intestinal epithelial tissue damage. J Clin Invest 2022; 132: e154993.
[29] Vereecke L, Vieira-Silva S, Billiet T, van Es JH, Mc Guire C, Slowicka K, Sze M, van den Born M, De Hertogh G, Clevers H, Raes J, Rutgeerts P, Vermeire S, Beyaert R and van Loo G. A20 controls intestinal homeostasis through cell-specific activities. Nat Commun 2014; 5: 5103.
[30] Yi PS, Shu Y, Bi WX, Zheng XB, Feng WJ, He LY and Li JS. Emerging role of zinc finger protein A20 as a suppressor of hepatocellular carcinoma. J Cell Physiol 2019; 234: 21479-21484.
[31] Feng Y, Zhang Y, Cai Y, Liu R, Lu M, Li T, Fu Y, Guo M, Huang H, Ou Y and Chen Y. A20 targets PFKL and glycolysis to inhibit the progression of hepatocellular carcinoma. Cell Death Dis 2020; 11: 89.
[32] Lee JH, Jung SM, Yang KM, Bae E, Ahn SG, Park JS, Seo D, Kim M, Ha J, Lee J, Kim JH, Kim JH, Ooshima A, Park J, Shin D, Lee YS, Lee S, van Loo G, Jeong J, Kim SJ and Park SH. A20 promotes metastasis of aggressive basal-like breast cancers through multi-monoubiquitylation of Snail1. Nat Cell Biol 2017; 19: 1260-1273.
[33] Guo T, Zhang Y, Qu X, Che X, Li C, Fan Y, Wan X, Ma R, Hou K, Zhou H, He X, Hu X, Liu Y and Xu L. miR-200a enhances TRAIL-induced apoptosis in gastric cancer cells by targeting A20. Cell Biol Int 2018; 42: 506-514.
[34] Guo W, Ma J, Guo S, Wang H, Wang S, Shi Q, Liu L, Zhao T, Yang F, Chen S, Chen J, Zhao J, Yu C, Yi X, Yang Y, Ma J, Ni Q, Zhu G, Gao T and Li C. A20 regulates the therapeutic effect of anti-PD-1 immunotherapy in melanoma. J Immunother Cancer 2020; 8: e001866.

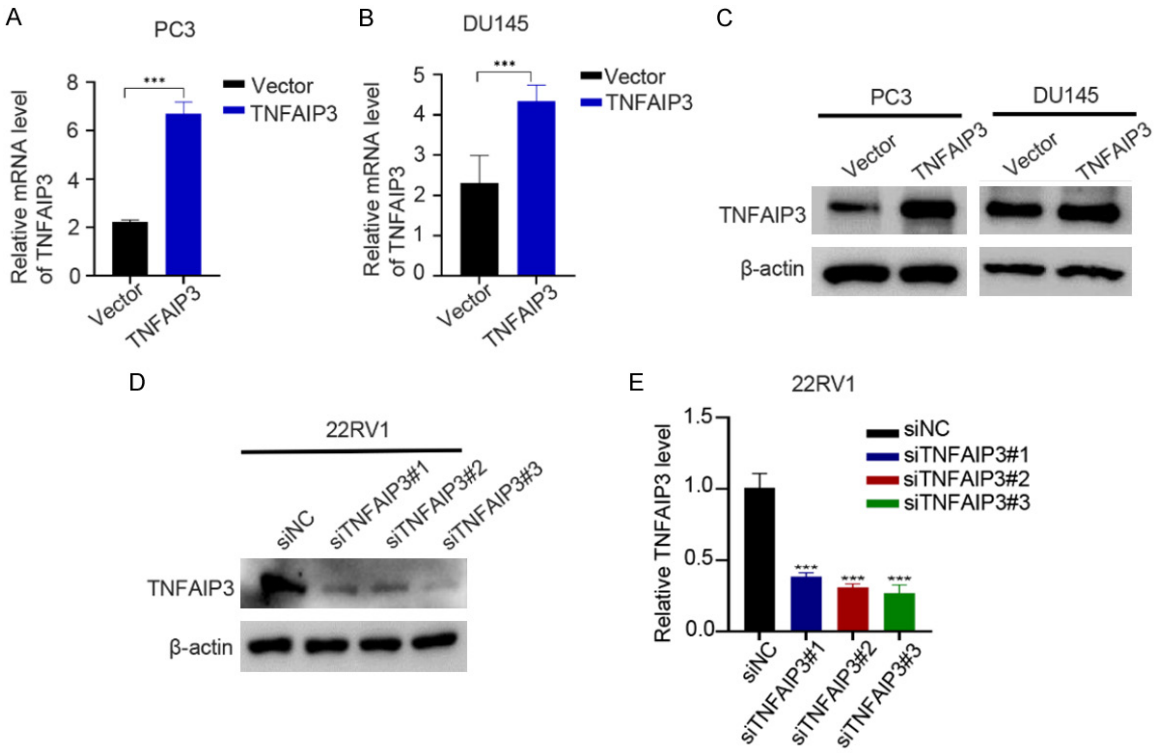

Figure S1. The transfection efficiency of TNFAIP3 in PCa cells was verified. A-C. The transfection efficiency of TNFAIP3 in PC3 and DU145 cells transfected with overexpression of TNFAIP3 were determined using qPCR and Western blot. D, E. The transfection efficiency of TNFAIP3 in 22RV1 cells transfected with siTNFAIP3 were determined using qPCR and Western blot. ***, P < 0.001.

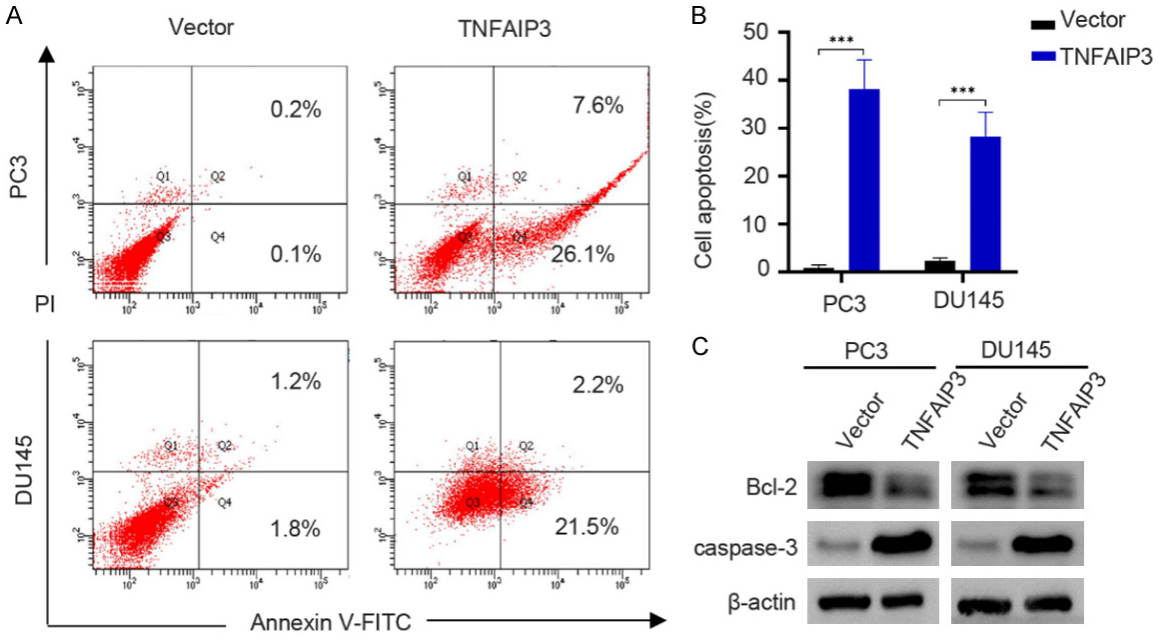

Figure S2. Overexpression of TNFAIP3 induces apoptosis in PC3 and DU145 cell lines. A, B. Cell apoptosis assays of PC3 and DU145 cells transfected with over-expression of TNFAIP3 using flow cytometry. C. Western blot analyses of caspase-3 and Bcl-2 in PC3 and DU145 cells after transfection with over-expression of TNFAIP3. ***, P < 0.001.